Acta Cryst. (1997). B53, 95–101

'Inverted Twinning' in Intergrowth Tungsten Bronzes

LARS KIHLBORG* AND MARGARETA SUNDBERG

Inorganic Chemistry, Arrhenius Laboratory, Stockholm University, S10691 Stockholm, Sweden. E-mail: larsk@inorg.su.se

(Received 24 June 1996; accepted 17 September 1996)

Abstract

A new type of twinning occurring in intergrowth tungsten bronzes (ITB) is described, revealed by high-resolution electron microscopy. Across the twin boundary the two structure elements of hexagonal tungsten bronze- and tetragonally distorted ReO_3-types are interchanged and grow in strict geometrical relationship to each other. The structure is thus 'inverted' and in the general case the two 'twin' parts represent different members of the structure family. Some members remain invariant upon inversion, however. This defect is most often seen as ribbons in an ITB matrix in Mo-doped samples $Cs_xMo_yW_{1-y}O_3$, which require a lower synthesis temperature than pure tungsten bronzes. They may be frozen-in stages of a slow ordering process. A similar type of twinning might be found in other intergrowth structures.

1. Introduction

It is well known that a two-dimensional net of regular octahedra of the type occurring in the hexagonal tungsten bronze (HTB) structure (Magnéli, 1953; Fig. 1*a*) fits perfectly to a net of ReO_3-type ($D0_9$), which is tetragonally distorted by a 15° tilt of the octahedra in an alternating sense around a common axis (Fig. 1*b*). This structure element will, for the sake of convenience, be abbreviated as TTO below. A perfect intergrowth of these two types of structure elements is then possible, which is realized in the *intergrowth tungsten bronzes*, ITB (Hussain & Kihlborg, 1976). These are built up of two-dimensionally infinite slabs of HTB and TTO, stacked along the third direction to form a three-dimensional network of corner-sharing octahedra, exemplified in Fig. 2. The structures were originally deduced from electron micrographs, but a confirmation and refinement of one member was later made by single-crystal X-ray diffraction methods (Hussain, 1977).

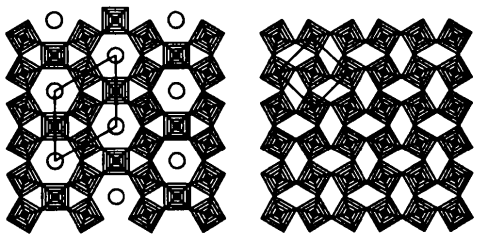

(*a*) (*b*)

Fig. 1. (*a*) The idealized structure of HTB depicted as corner-linked octahedra forming hexagonal tunnels, which are fully or partly occupied by large atoms, *i.e.* K, Rb and Cs (drawn as circles). (*b*) An ReO_3-type structure in which the octahedra have been tilted by 15° in an alternating sense around an axis perpendicular to the plane of the paper. This tetragonal structure, abbreviated as TTO in this paper, fits perfectly the $\{10\bar{1}0\}$ planes in HTB.

Like all tungsten bronzes, the ITB's have the general formula A_xWO_3 and the A atoms, typically the larger alkali atoms K, Rb and Cs, occupy the hexagonal tunnels in the HTB elements. As with all intergrowth structures, an infinite number of ordered homologous structures can be proposed, differing in the widths of the two types of slabs. It has been found useful to designate the different members of this structure family by numerals, indicating the number of complete rows of octahedra between the centres of the hexagonal tunnels, enclosing the repeating sequence by parentheses, as exemplified in Fig. 2.

In the A_xWO_3 system the intergrowth tungsten bronzes form only at 1075 K and above, for x values in the range $x \simeq 0.05$–0.10 (Hussain, 1978). The identified phases include the members $(1,n)$, with n values ranging from 4 to 14 (Kihlborg, Fernandez, Laligant & Sundberg, 1988). These contain HTB elements that are two tunnel rows wide and seem to be particularly stable in this system. Single tunnel structures, designated n, have also been found, with n values ranging from 7 to 11 (Kihlborg, 1979). Disorder is frequently encountered, ranging from the case where a single slab of deviating width occurs in an otherwise periodic structure, to structures where the widths of both elements vary in a random fashion.

Tungsten in ITB may be partly replaced by a pentavalent transition metal, giving rise to fully oxidized phases, with the general formula $A_xT_xW_{1-x}O_3$, which have been termed *bronzoids* since they have the same structures but lack the physical and chemical properties of the true bronzes. The preparation temperature has to be higher in this case, 1175 K for V and 1475 K for Nb and Ta (Sharma & Kihlborg, 1981; Sharma, 1985). In these ITB systems, with nominal $x \simeq 0.1$, ordered structures with HTB slabs two, three, four and five tunnel rows wide and TTO slabs containing two–nine octahedra across have been observed (Kihlborg & Sharma, 1982).

© 1997 International Union of Crystallography
Printed in Great Britain – all rights reserved

The HTB-type elements thus seem more stable in these substituted phases. Also, Ti may be substituted for tungsten (Sharma, 1985).

We have recently found that also molybdenum can replace tungsten in the ITB bronzes. ITB crystals $A_xW_{1-y}Mo_yO_3$ with y as high as 0.60, as measured by EDS microanalysis, have been prepared. These studies have so far been limited to the K and Cs bronzes (Ringaby & Sundberg, 1995; Kihlborg, Norrby & Sundberg, 1995). The synthesis temperature can be lower when Mo is present and the solid-state reaction between the actual oxides is reasonably complete after a few days even at 925 K. The ITB members formed are mostly (1,n) phases, with n ranging from 3 to 6, but also triple-tunnel, as in (1,1,3)-ITB, and single-tunnel structures, such as (4)-ITB, have been observed (Kihlborg, Norrby & Sundberg, to be published).

High-resolution electron microscopy, HREM, has revealed a particular type of twinning in some of these Mo-substituted ITB crystals, which is reported below.

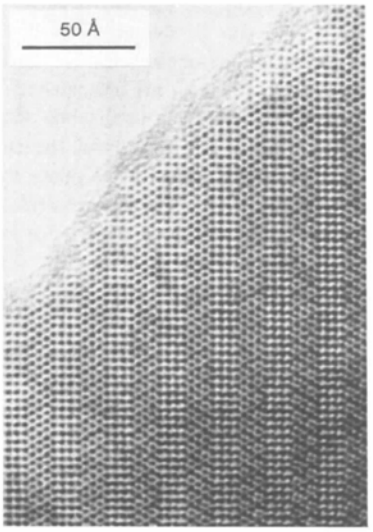

(*a*)

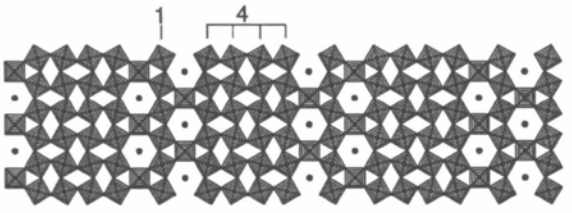

(*b*)

Fig. 2. The structure of (1,4)-ITB. (*a*) HREM image, where all metal atoms are well resolved. (*b*) Corresponding structure model. The MO_6 octahedra are simply stacked by sharing corners along the line of sight (c axis). The alkali atoms in the tunnels are indicated as small black circles here, but they are not marked in the models that follow. The complete vertical rows of octahedra between the (centres of) HTB tunnels in one repeat sequence are marked. The numbers of these are used for the designation of the various ITB phases.

2. Experimental

The results reported here were obtained essentially from three samples, prepared by heating weighed, carefully ground mixtures of WO_3, Cs_2WO_4, MoO_3 and WO_2 in sealed silica tubes under the following conditions:

Sample (I): nominal composition $Cs_{0.08}(Mo_{0.08}W_{0.92})O_3$; 6^d, 1000 K + 16^d, 925 K;

Sample (II): nominal composition $Cs_{0.07}(Mo_{0.11}W_{0.89})O_3$; 11^d, 925 K + 14^d, 1000 K;

Sample (III): nominal composition $Cs_{0.08}(Mo_{0.49}W_{0.51})O_3$; 5^d, 1010 K.

TEM specimens were prepared by gentle crushing of the samples in a mortar, dispersing the powder in n-butanol, transferring a drop to a holey carbon film supported by a Cu grid and letting the liquid evaporate. ED patterns were recorded in a JEOL 2000FX transmission electron microscope equipped with a LINK AN10000 EDS microanalysis system. The W M, Mo K and Cs L peaks from thin parts of the crystals were used for quantitative evaluation of the composition using the thin specimen approximation method. HREM images were taken in a JEOL JEM-200CX microscope ($\pm 10°$ double-tilt top-entry stage) at 200 kV and in a JEM-3010 microscope (URP31 pole-piece, double-tilt, side-entry stage) at 300 kV.

3. Results

The samples were multiphasic, but ITB was the majority phasoid (a term introduced by Magnéli, 1986). (1,5)-ITB was the dominating member in samples (I) and (II), but also (4)-, (1,4)- and (1,6)-ITB crystals were identified. Microanalysis of the same crystals showed that the Cs content was close to the nominal, but the Mo content was only 50–75% of the bulk composition. Analysis of sample (III) indicated that the crystals were mainly (1,3)- and (1,4)-ITB with $x = 0.12$–0.15 and $y \simeq 0.45$ in $Cs_xMo_yW_{1-y}O_3$.

Fig. 3(*a*) shows an HREM image of a crystal fragment from sample (I). The crystal is predominantly (1,5)-ITB and three parts, marked *A*, *B* and *C*, can clearly be distinguished in this image. In part *B* there is a defect (indicated), where the intergrowth sequence is (...1,5,1,3,1,1,5,1...) instead of just (1,5), *i.e.* one TTO slab is only three octahedra wide, while the neighbouring HTB element contains three tunnel rows, as shown in Fig. 3(*b*). Parts *A* and *C* are in parallel orientation, although shifted laterally, while part *B* is rotated by 30° with respect to the other two. There are two boundaries between *B* and *C*. That marked *bc*1 is a true twin boundary running along {110} and relating the two individuals by a glide operation. The two structure elements are thereby interchanged 'inverted' across the boundary so that an HTB slab in one part continues as a TTO slab, inclined 30°, in the other and *vice versa*. We call this type of twinning 'inverted twinning', which results from the joining of TTO and HTB elements along

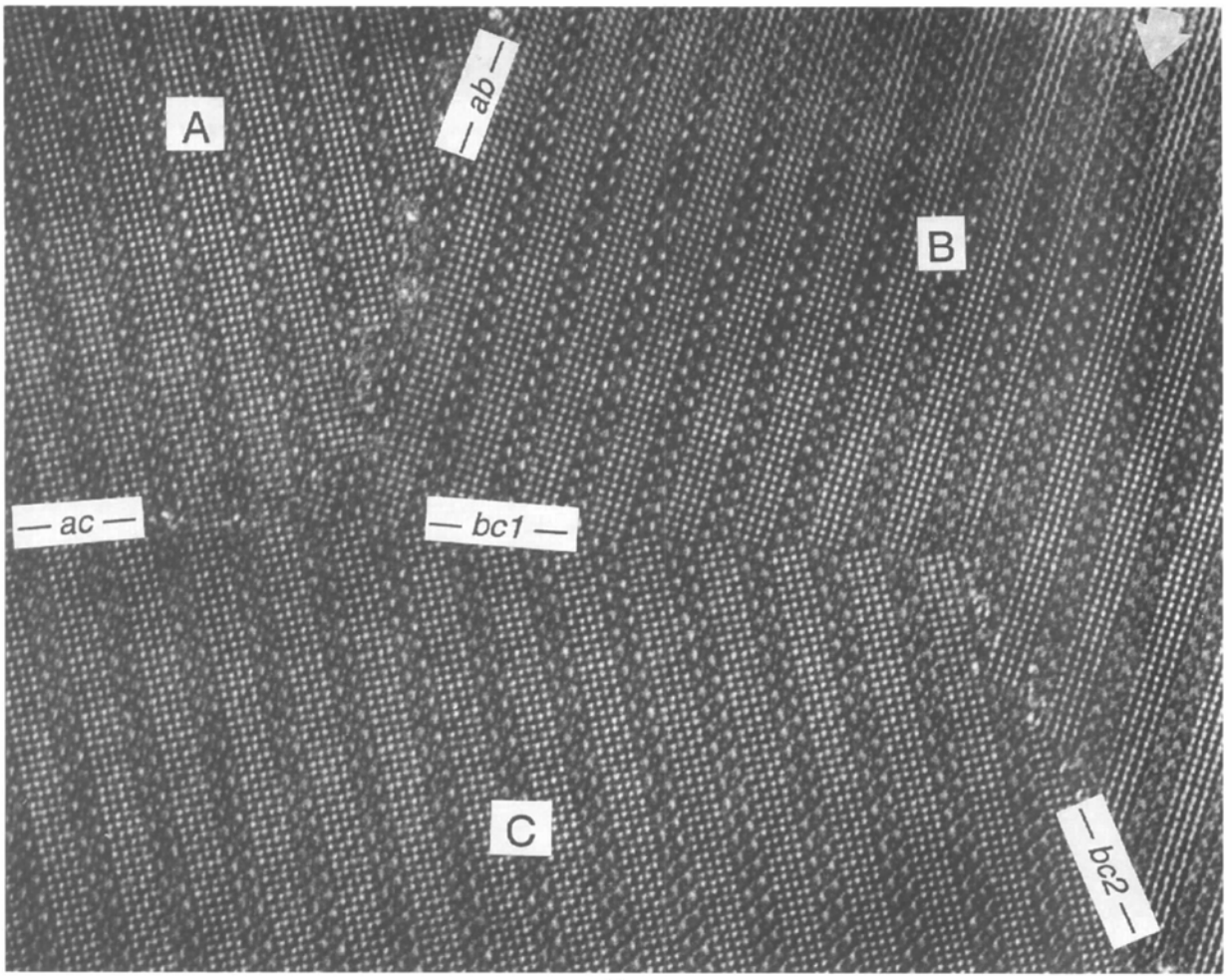

(*a*)

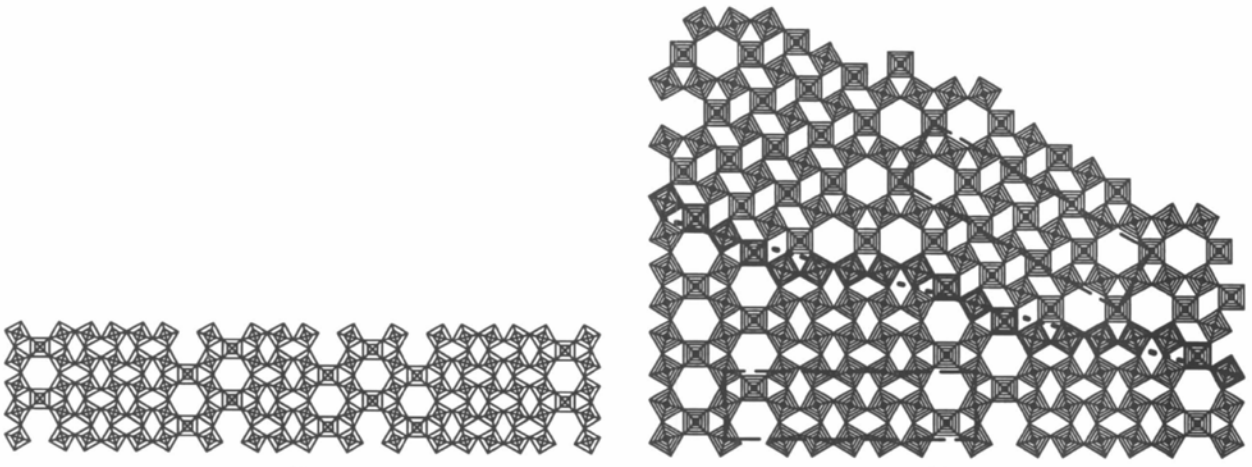

(*b*) (*c*)

Fig. 3. (*a*) HREM image of a crystal fragment of relatively well-ordered (1,5)-ITB from sample (I). Three different areas, marked by capital letters, can be distinguished. There is a local defect with deviating intergrowth sequence in region *B* (marked by an arrow; model in *b*). The crystal is relatively thick in the part shown, which lowers the interpretable resolution, but the HTB and TTO slabs are clearly revealed. The boundary marked *bc*1 is an inverted twin boundary, where HTB twins into TTO and *vice versa*. (*b*) A model of the irregular ITB sequence (1,5,1,3,1,1,5,1) seen as a defect in *a*. (*c*) Model of 'inverted twinning' in (1,5)-ITB. The unit cells (long axis: *a*; short axis: *b*) and the twin plane along (110) are indicated. The octahedra which are common to both individuals are heavily outlined. In this case the structure is the same on both sides of the boundary.

the second of the three equivalent $\{10\bar{1}0\}$ planes in the hexagonal HTB structure. The resulting boundary is completely coherent; the octahedra along this boundary are common to both structure elements, as the model in Fig. 3(*c*) shows.

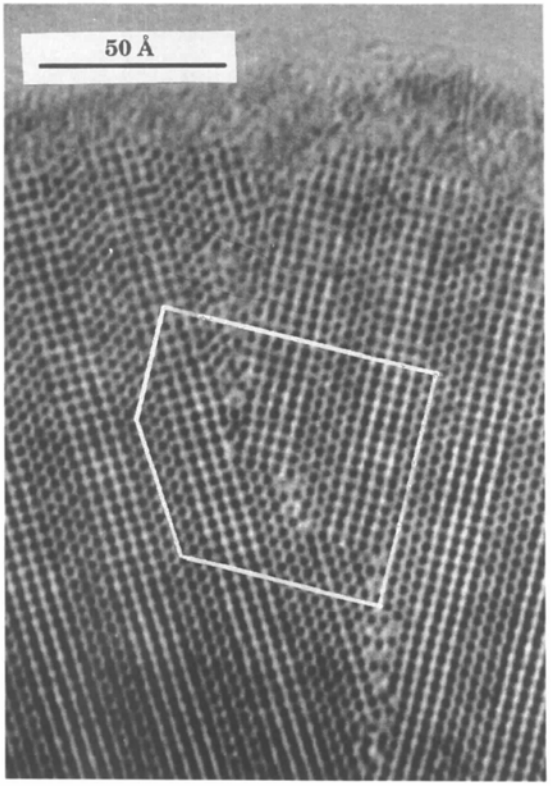

(*a*)

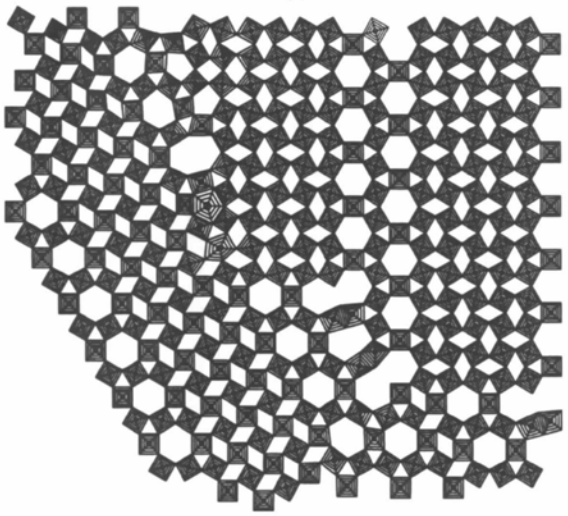

(*b*)

Fig. 4. (*a*) Part of the same crystal as in Fig. 3 close to the edge, showing the *ab* boundary at atomic resolution. (*b*) A model of the indicated area of *a*, in terms of MO_6 octahedra and MO_7 pentagonal bipyramids (known from other tungsten and molybdenum oxides). The Cs atoms in the tunnels are not indicated.

The boundaries marked *bc*2 and *ab* are running in other directions, in which the structures do not match completely, although the strict geometrical relation between the areas on both sides is maintained. While there is still HTB/TTO inverted twinning locally between pairs of slabs, it does not extend laterally and the structure at these boundaries has to adjust itself to the best fit, which gives rise to wider tunnels, revealed as areas with lighter contrast in the images. A part of the *ab* boundary further up, close to the edge, is shown in Fig. 4(*a*). Here, the crystal is so thin that the individual metal atoms are clearly resolved and the structure along part of the boundary can be modelled (Fig. 4*b*). Interpretation in terms of octahedra and pentagonal bipyramids linked in various ways (found in other tungsten oxides) is thus straightforward. Along the *ac* boundary the structure is shifted laterally by two octahedral rows, while three rows of octahedra in the TTO parts continue almost straight across the boundary. Such a shift cannot take place without structure rearrangement at the boundary and this is also shown in the image, although this part does not have clear atomic resolution. A tentative model of this boundary is shown in Fig. 5.

3.1. *Inverted twinning in ITB*

As shown above the inverted twinning of (1,5)-ITB gives rise to the same structure on both sides. This is a special case. It is seen in Fig. 6 that a single-HTB-tunnel row twins into a TTO element three octahedra wide, a double-tunnel row into one which is five octahedra wide *etc.*, adding two TTO rows for each HTB tunnel row. Thus, only TTO slabs that have an odd number of octahedra across can have an HTB twin counterpart. Some examples of ITB structures that are related by inverted twinning are given in Table 1. The general formula for the inverted twin relation, in terms of the designation of the ITB members described above, is

$$\begin{array}{ccc} (1,1,\ldots,n) & \longleftrightarrow & (1,1,\ldots,2R+1). \\ R & & (n-1)/2 \end{array}$$

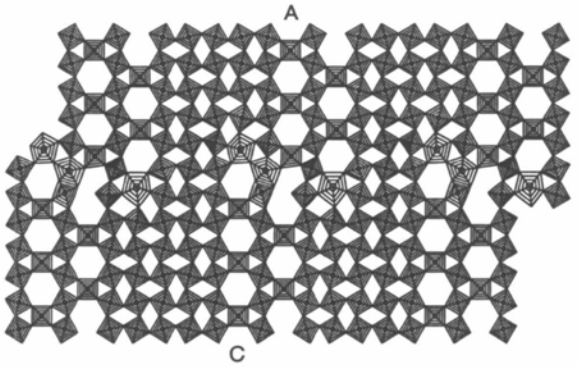

Fig. 5. A tentative model of the boundary marked *ac* in Fig. 3(*a*), across which the structure is shifted laterally by two octahedra.

(We are here considering only the simplest case of intergrowth where all slabs of HTB have the same width and the same is true for the TTO slabs.) The lower line indicates the number of items separated by commas within the parentheses, which equals the multiplicity of the tunnel rows in the HTB elements, and thus their width. The last items within the parentheses, n and $2R+1$, indicate the number of octahedral rows in the TTO slabs.

The ITB structures that are indicated in bold type in Table 1 are inverted into themselves by the twinning. In these cases the composition need not change. This is not the case for the other inverted twin pairs, where the relative proportion of tunnels is different. This gives different values of x_{max}; thus, the alkali content or the tunnel occupancy have to change across the border.

3.2. *Inverted twin ribbons inside ITB crystals*

Large twin areas such as those shown in Fig. 3(*a*) have not often been found. More frequent are defects in the form of ribbons of inversely twinned ITB, such as those shown in Fig. 7. Such a ribbon will shift the structure sidewise, the displacement being proportional to its thickness; one octahedral row for every two octahedra in width. A twin ribbon in (1,5)-ITB (Fig. 7) will run

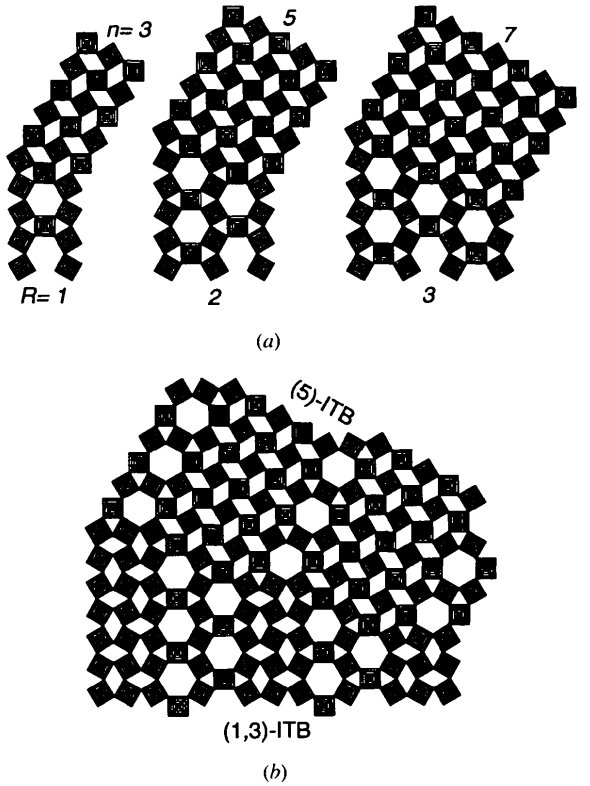

Fig. 6. (*a*) Octahedral models showing how HTB slabs, R tunnel rows wide, change into TTO slabs $2R+1$ octahedra across, inclined 30° to the tunnel rows. (*b*) Model of inverted twinning of (1,3)-ITB into (5)-ITB.

Table 1. *Examples of inverted twin counterparts*

R indicates tunnel multiplicity in the HTB element. x_{max} is the alkali content in A_xMO_3 with full tunnel occupancy. Structures in bold are invariant by the twinning.

ITB	R	x_{max}	ITB	R	x_{max}
(3)	1	0.143	(3)	1	0.143
(5)	1	0.091	(1,3)	2	0.200
(7)	1	0.067	(1,1,3)	3	0.231
(1,5)	2	0.143	**(1,5)**	2	0.143
(1,7)	2	0.111	(1,1,5)	3	0.176
(1,9)	2	0.091	(1,1,1,5)	4	0.200
(1,1,7)	3	0.143	**(1,1,7)**	3	0.143
(1,1,9)	3	0.120	(1,1,1,7)	4	0.167
(1,1,1,9)	4	0.143	**(1,1,1,9)**	4	0.143

in a direction inclined 75° (or 105°) to the tunnel rows and the ribbon will have the same structure, thus the composition need not be changed. In (1,3)-ITB (Figs. 8 and 9) the twin ribbon will have the (5)-ITB structure and run in a direction close to 70° (or 110°) to the tunnel rows (*b* axis) in the matrix. The twin ribbon seen in Fig 8 is narrow, only three octahedra wide. This is not unexpected in view of the difference in structure, and thus in composition, of the two twin counterparts. Fig. 9 shows an inverted twin defect which separates a well ordered region of the crystal and one that shows extensive variation in width of both the HTB and TTO slabs.

4. Discussion

'Inverted twinning' might occur in other types of intergrowth structures. The concept could be useful whenever there is a strict geometrical relationship between two parts of a crystal having an intergrowth structure with a boundary (inclined to the intergrowth planes), across which the components are interchanged and the structure inverted (Fig. 10). It gives an anti-phase relation between two regions, but the mechanism includes a twin operation, which is why it seems appropriate to give it a special name. 'Anti-phase twinning' would be an alternative, but we prefer 'inverted twinning' (not to be confused with 'inversion twin', a well known term in crystallography).

In the light of the discovery of this particular type of twinning in Mo-substituted samples, some old HREM images of unsubstituted ITB crystals were also examined and the same type of twinning was occasionally found as local defects. The resolution in these older images was not such that an unequivocal identification without the present information could have been made, however. The phenomenon is thus not restricted to substituted samples, but is a general defect feature in ITB phases.

Although occasionally also found in undoped ITB crystals, inverted twinning seems much more frequent in the Mo-doped samples. It is possible that the lower temperature used in the synthesis of the Mo-doped

samples favours the occurrence of these defects, which may more easily anneal out at higher temperatures. As a matter of fact it is often seen that the structure is more ordered on one side of a twin ribbon than on the other (Fig. 9), which may suggest that they play a role in the ordering mechanism and are frozen-in stages of an ordering process. The observation that the crystals from sample (III), which has the shortest annealing time,

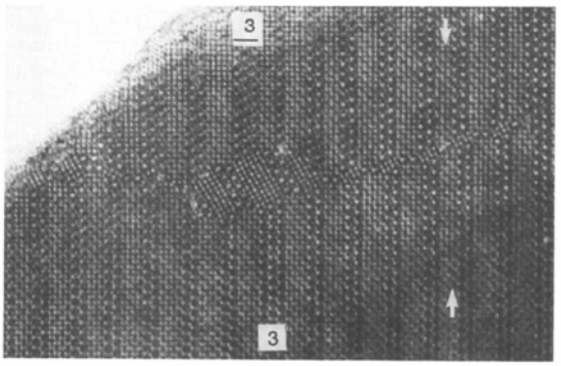

(*a*)

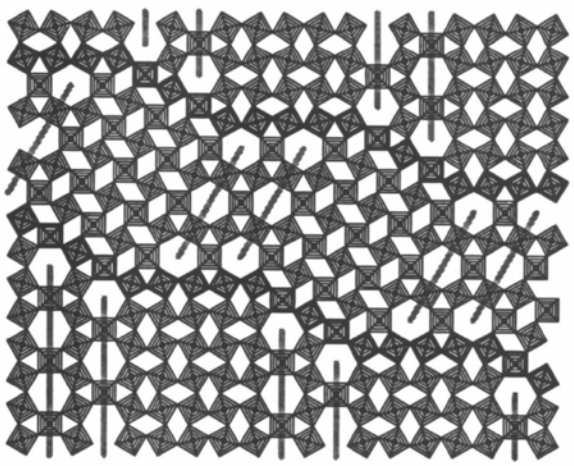

(*b*)

Fig. 7. (*a*) HREM image of an inverted twin defect in a matrix which is rather disordered but predominantly (1,5)-ITB [from sample (II)]. To the right, a twin ribbon two-octahedra thick shifts the structure sideways by two octahedra. One TTO slab in both the upper and lower part is only four octahedra wide (marked by arrows). This requires a modified structure of the ribbon since TTO slabs with an even number of octahedra (n) across do not have an inverted twin counterpart. An abnormal white contrast is also seen there. In the centre the twin area widens. It is clearly seen how a triple-tunnel HTB slab (marked '3') is invertedly twinned into a TTO slab, seven octahedra wide. There are abnormal features also here, which, however, elude a detailed interpretation due to the rather large thickness of the crystal. (*b*) A model of an inverted twin ribbon (in this case seven octahedra thick, including the octahedra which are common to both parts) inserted into a (1,5)-ITB matrix, shifting the structure sideways. (Here the shift corresponds to three octahedra.) The directions of the tunnel rows have been emphasized by grey lines.

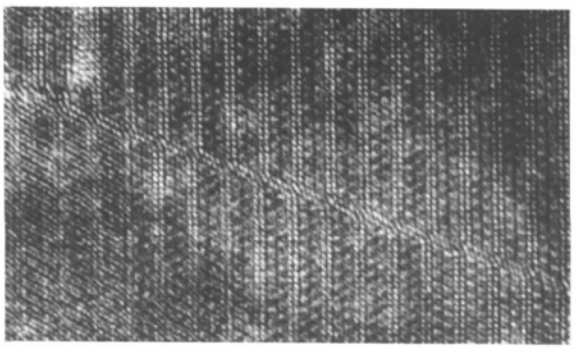

(*a*)

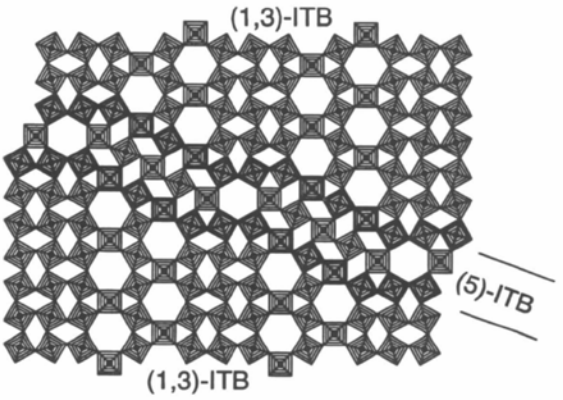

(*b*)

Fig. 8. (*a*) An HREM image of a (1,3)-ITB crystal [sample (III)], showing an inverted twin ribbon of (5)-ITB, two octahedra wide, shifting the structure laterally by one octahedral row. The TTO slabs appear as rows of white dots (the space between the metal atoms) in this image. (*b*) Model of this twin structure.

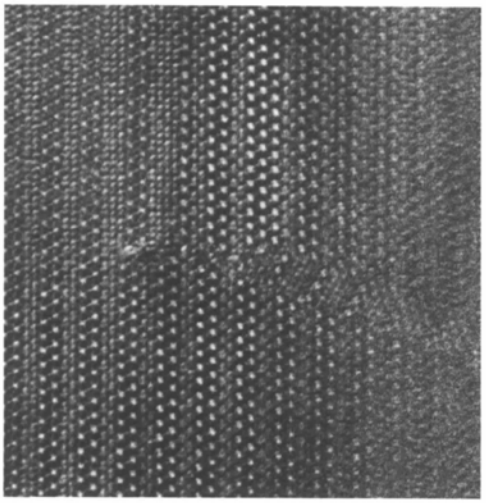

Fig. 9. An HREM image of a crystal [also from sample (III)] being largely (1,3)-ITB, but showing extensive disorder in the upper part. An inverted twin ribbon, essentially (5)-ITB, starts in the middle and extends to the right. The HTB tunnels appear bright in the central part, but become dark in the thick region to the right. The crystal is well ordered below the twin.

seems to be more defect-rich than those from the other two samples speaks in favour of this.

These defects are generally observed in thicker parts of the crystal fragments, which are unfavourable for a direct interpretation of the HREM images. Fragments with large thin twin areas, such as that in Fig. 3(*a*), are rare. This may, at least partly, be due to the unsophisticated specimen preparation method used; when crushed the crystals should be apt to fracture along the twin boundaries, particularly if these are not running in the ideal crystallographic direction. Thus, it is to be expected that fracture should easily occur along such boundaries as those designated *ab*, *ac* and *bc*2 in Fig. 3(*a*).

Extensive twinning of the non-invariant type has not been observed so far and is likely to be less favourable for stoichiometric reasons. Such twinning implies either different alkali content of the two counterparts or rather different tunnel occupancy, as seen from Table 1, where x_{max} indicates the alkali content when the tunnels are completely filled. We normally find a rather narrow distribution of x in crystals from the same sample and if the sample contains different ITB members, the x values from the analyses are generally such that they correspond to approximately the same degree of tunnel occupancy. Large variations in the degree of filling are thus not likely within the same sample.

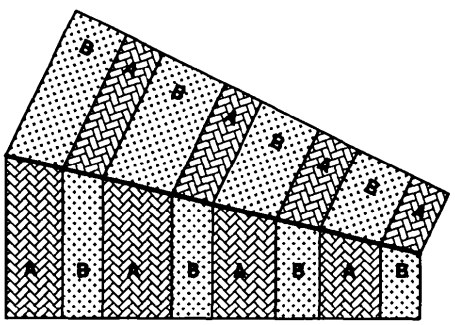

Fig. 10. Schematic drawing of inverted twinning in a general intergrowth structure *ABAB*. The two components *A* and *B* are interchanged across the twin boundary (heavy line).

This investigation forms part of a research project financially supported by the Swedish Natural Science Research Council.

References

Hussain, A. (1977). *Chem. Scr.* **11**, 224–227.
Hussain, A. (1978). *Chem. Commun. Univ. Stockholm*, No. 2, 1–44.
Hussain, A. & Kihlborg, L. (1976). *Acta Cryst.* A**32**, 551–557.
Kihlborg, L. (1979). *Chem. Scr.* **14**, 187–196.
Kihlborg, L. & Sharma, R. (1982). *J. Microsc. Spectrosc. Electron.* **7**, 387–396.
Kihlborg, L., Fernandez, M., Laligant, Y. & Sundberg, M. (1988). *Chem. Scr.* **28**, 71–75.
Kihlborg, L., Norrby, L.-J. & Sundberg, M. (1995). *Extended Abstracts*, pp. 95–96. 47th SCANDEM Meeting, Trondheim, Norway.
Kihlborg, L., Norrby, L.-J. & Sundberg, M. (1997). To be published.
Magnéli, A. (1953). *Acta Chem. Scand.* **7**, 315–324.
Magnéli, A. (1986). *Chem. Scr.* **26**, 535–546.
Ringaby, O. & Sundberg, M. (1995). *Abstracts*, No. P25-02, p. 152. 16th European Crystallographic Meeting. Lund, Sweden.
Sharma, R. (1985). *Chem. Commun. Univ. Stockholm*, No. 3, 1–42.
Sharma, R. & Kihlborg, L. (1981). *Mater. Res. Bull.* **16**, 377–380.